

1 Chapter 1

2 The FEniCS Project on AWS Graviton3

3 M. Habera and J. S. Hale

4 **Abstract** ARM architecture central processing units are increasingly prevalent in
5 high performance computers due to their energy efficiency, scalability and cost-
6 effectiveness. The overall goal of this study is to evaluate the suitability of ARM-
7 based cloud computing instances for executing finite element computations. Specif-
8 ically, we show performance results executing the FEniCS Project finite element
9 software on Amazon Web Services (AWS) *c7g* and *c7gn* instances with Graviton3
10 processors. These processors support ARMv8.4-A instruction set with Scalable Vec-
11 tor Extensions (SVE) for Single Instruction Multiple Data operations and the Elastic
12 Fabric Adaptor for communications between instances. Both clang 18 and GCC
13 13 compilers successfully generated optimized code using SVE instructions which
14 ensures that users can achieve optimized performance without extensive manual
15 tuning. Testing a distributed memory parallel DOLFINx Poisson solver with up
16 to 512 Message Passing Interface processes, we found that the performance and
17 scalability of the AWS instances are comparable to a dedicated AMD EPYC Rome
18 cluster installed at the University of Luxembourg. These findings demonstrate that
19 ARM-based cloud computing instances, exemplified by AWS Graviton3, can be
20 competitive for distributed memory parallel finite element analysis.

21 Introduction

22 The FEniCS Project (Alnæs et al., 2015; Baratta et al., 2023b) has been used to write
23 finite element solvers for problems arising in fields that involve the solution of partial

M. Habera e-mail: michal.habera@rafinex.com

Rafinex SARL, Luxembourg and Institute of Computational Engineering, Department of Engineer-
ing, Faculty of Science, Technology and Medicine, University of Luxembourg, Luxembourg.

J. S. Hale e-mail: jack.hale@uni.lu

Institute of Computational Engineering, Department of Engineering, Faculty of Science, Technol-
ogy and Medicine, University of Luxembourg, Luxembourg.

24 differential equations (PDEs), including mathematics, biology, physics, engineering,
25 geophysics and mechanics.

26 Exploring ARM-based processors and cloud computing instances for executing FEn-
27 iCS Project-based solvers is worthwhile due to ARM's potential advantages in cost-
28 effectiveness, energy efficiency and scalability with respect to x86-64-based ma-
29 chines (Simakov et al. (2023); Suárez et al. (2024)). Examples of adoption of ARM
30 in the HPC space include the Isambard project (Isambard 3, NVIDIA Grace, (BCS,
31 2025)), Mont-Blanc project (Phase 3, Cavium Thunder X2, (Rajovic et al. (2016)),
32 Fugaku supercomputer (Fujitsu A64FX, (Fujitsu, 2024)) and Astra supercomputer
33 (Cavium Thunder X2, (Sandia, 2018)). The publically available cloud services with
34 ARM instances include Amazon Web Services (AWS) (Graviton3 CPU based on
35 Neoverse V1 and Graviton4 CPU with Neoverse V2), Google Cloud (Axion CPU
36 based on Neoverse V2, (Google, 2025)) and Microsoft Azure (Azure Cobalt 100
37 based on Neoverse N2, (Microsoft, 2024)).

38 AWS Graviton3-based instances aim to provide cost effective compute resources for
39 scientific computing and machine-learning applications by including both Scalable
40 Vector Extension (SVE) instructions for Single Instruction Multiple Data (SIMD)
41 parallelism and the Elastic Fabric Adaptor (EFA) interconnect for high-bandwidth
42 low-latency communication between instances. This makes the AWS cloud offering
43 particularly appealing for executing scientific computing codes, like the FEniCS
44 Project.

45 A key technology in the FEniCS Project is the use of automatic code genera-
46 tion (compilation). The user expresses their finite element problem in the Unified
47 Form Language (UFL) (Alnæs et al. (2014)) and then the FEniCSx Form Compiler
48 (FFCx) (Kirby and Logg (2006)) compiles the UFL description of the problem into a
49 low-level C kernel for computing the cell-local finite element tensor.

50 One aspect of good performance of a compute-bound kernel is ensuring the assembly
51 code of the compiled kernel contains calls to Single Instruction Multiple Data
52 (SIMD) operations. SIMD operations can apply the same operation to multiple data
53 items in a single CPU clock cycle. For a recent overview of SIMD programming
54 strategies see e.g. (Rocke (2023)). The current strategy of FFCx with respect to
55 SIMD is to ensure that its kernels are amenable to the compiler applying automatic
56 vectorisation, a process that automatically converts a scalar program into a vectorised
57 equivalent that uses SIMD operations.

58 Consequently for users to achieve good performance when using FEniCSx on Gravi-
59 ton3 it is important to verify that the latest compilers do automatically emit SVE
60 and/or Neon SIMD instructions when compiling the generated C finite element
61 kernels and that these kernels achieve reasonable runtime performance.

62 In addition to SIMD parallelisation at the kernel level, DOLFINx, the finite ele-
63 ment problem solving environment of the FEniCS Project, also supports distributed
64 memory parallel assembly of global finite element data structures (sparse matrices
65 and vectors) using the Message Passing Interface (MPI), for full details see (Baratta

66 et al. (2023b). For user's to run large-scale DOLFINx simulations on AWS it is
 67 necessary to verify that the EFA interconnect provides sufficient performance for
 68 parallel scalability.

69 In summary, the contribution of this chapter is to examine both SIMD performance
 70 and multi-node parallel scaling of the FEniCS Project software on Amazon's Gravi-
 71 ton3 based instances.

72 Methodology and Results

73 Systems

74 AWS c7g and c7gn instances are compared to Aion computing instances available at
 75 the University of Luxembourg HPC facilities (Varrette et al. 2022). These instances
 76 have different hardware configuration, see Table 1.1 for full details.

77 The FEniCS Project components are written in a mixture of Python, modern-style
 78 C++20 and Standard C17. The Python interface is a wrapper around the core data
 79 structures and computationally intensive algorithms written in C and C++.

	Aion node	AWS c7g instance
Processor	2 x (AMD Epyc ROME 7H12, 64 cores @ 2.6 GHz)	1 x (Graviton3, 64 cores @ 2.6 GHz)
Architecture	x86_64, Zen 2 (AVX2)	ARMv8.4-A, Neoverse V1 (SVE)
Memory	256 GB DDR4 3200 MT/s = 25.6 GB/s 8 NUMA nodes	128 GB DDR5 4800 MT/s = 38.4 GB/s Unified Memory Access (no NUMA)
Total mem. bandwidth	2 x 200 GB/s	1 x 300 GB/s

Table 1.1: Configuration of the Aion nodes (University of Luxembourg HPC) and AWS c7g (Amazon) instances. The c7gn instance used in the Poisson weak scaling test has the same hardware as c7g with the addition of a 200 GB s^{-1} interconnect between instances for MPI-based communication.

80 Memory bandwidth

81 Low-order finite element methods are typically memory bandwidth constrained as
 82 the time taken to load and store data from main memory (e.g. the mesh geometry)
 83 dominates the time taken to perform the arithmetic operations to compute the fi-

84 nite element cell tensor. Understanding the memory bandwidth characteristics of a
 85 processor is therefore important for ensuring optimal performance.

86 STREAM (McCalpin, 1995, 1991-2007) is the industry standard benchmark for mea-
 87 suring sustained memory bandwidth performance. They estimate memory bandwidth
 88 from memory intense operations (copy, scale, add) on large contiguous arrays.

89 In Figure 1.1 results for the copy operation for single-node benchmark are shown.
 90 For the single-node benchmark 80 % of the theoretical peak memory bandwidth of
 91 400 GB s^{-1} for Aion and 300 GB s^{-1} for AWS c7g is reached. This is considered a
 92 reasonable outcome of the STREAM benchmark, (McCalpin, 2023). Bandwidth sat-
 93 uration is observed at around 20 % of the node utilisation. Both curves show different
 94 characteristics of the saturation point due to different memory access configuration.
 95 On the Aion instances there are 8 non-unified memory access (NUMA) nodes of 16
 96 cores each, while AWS c7g instances are setup with unified memory access.

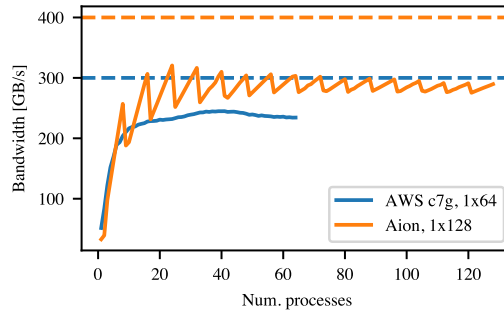


Fig. 1.1: Single-node STREAM benchmark. Theoretical peak bandwidth of each system show as dashed line.

97 Finite element kernels

98 In order to measure the performance of a standard FEniCS user finite element code
 99 we used the Local Finite Element Operator Benchmarks repository (Baratta et al.,
 100 2023a). The benchmark measures execution time for local finite element kernel
 101 generated by the FEniCS Form Compiler (FFCx) v0.9.0 (Kirby and Logg, 2006).
 102 We generate a matrix-free three-dimensional Laplace kernel representing a finite
 103 element discretisation of the action of Laplace operator A_{ij} with spatially varying
 104 material property $\kappa(x)$

$$v_i = A_{ij}w_j, \quad A_{ij} = \int_K \kappa J_{mk} J_{mn} \nabla_k \phi_i \nabla_n \phi_j |\det J| dx, \quad (1.1)$$

105 where K is a fixed reference tetrahedron, $w_j \in \mathbb{R}^n$ is a fixed, prescribed vector, J is
106 a Jacobian transformation matrix and ϕ are finite element basis functions.

107 The generated kernel calculates a double precision vector $v_i \in \mathbb{R}^n$, where $n = 4$
108 for first-order discretization (low-order) and $n = 165$ for eight-order discretization
109 (high-order). Low-order kernels are expected to be memory bandwidth limited,
110 while high-order kernels have higher arithmetic intensity. In addition, the matrix-
111 free (operator action) version requires fewer load and store operations in comparison
112 to the assembly of a matrix, increasing the ratio of floating-point operations to
113 memory loads and stores. Consequently for the high-order kernels there is the scope
114 for significant performance increases if the compiler can automatically emit SIMD
115 operations.

116 Generated code structure

117 Compiler (loop) SIMD auto-vectorisation is usually performed for inner-most loops
118 with compile-time known bounds. The analysis of FFCx autogenerated code is
119 required to understand the potential and missed optimisations.

Code Listing 1.1: Abbreviated FFCx generated finite element kernel.

```

120 void kernel(double* restrict A, const double* restrict w, ...){
121     // 1. Static arrays of basis functions and quadrature weights.
122     // 2. Quadrature rule independent computations.
123
124     for (int iq = 0; iq < NUM_QUAD_POINTS; ++iq) {
125         // 3. Quadrature loop body.
126         for (int ic = 0; ic < NUM_DOFS; ++ic){
127             // 3.1 Coefficient evaluation.
128             w1_d100 += w[4 + (ic)] * FE0_C0_D100_Q530[0][0][iq][ic];
129             // ...
130         }
131
132         // 3.2 Scalar graph evaluation.
133         double sv_530_0 = w1_d100 * sp_530_18;
134         double sv_530_1 = w1_d010 * sp_530_22;
135         // ...
136
137         for (int i = 0; i < NUM_DOFS; ++i) {
138             // 3.3 Tensor assignment loop.
139             A[(i)] += fw0 * FE0_C0_D100_Q530[0][0][iq][i];
140             // ...
141         }
142     }
143 }
144

```

146 An abbreviated example of generated C code is shown in Code Listing [1.1](#). Firstly,
147 there are arrays defining finite element basis functions at quadrature points. These
148 require no arithmetic operations. Computations independent of the quadrature loop
149 contain more intense arithmetic operations (e.g. determinant of the Jacobian), but
150 are executed only once. Non-affine geometry would require evaluation of geometric

151 quantities at each quadrature point, which would increase the arithmetic intensity
 152 and yield more opportunities for vectorisation.

153 The most performance critical part of the code is contained in the quadrature loop
 154 body. For the eight-order Laplace operator there is `NUM_QUAD_POINTS = 214` and
 155 `NUM_DOFS = 165`. There are two inner-most loops: coefficient evaluation and tensor
 156 assignment. Both contain a set of multiply-add operations which are candidates for
 157 automatic vectorisation via fused multiply-add operations in both SVE (Graviton3)
 158 and AVX2 (AMD EPYC).

159 Experimental results

160 For the finite element kernel benchmarks we compiled the kernels with LLVM/clang
 161 18.1.3 and GCC 13.2.0. Full details are given in [Table 1.2](#)

	Compiler	Aion	AWS c7g
Ofast, native, vectorized	GCC 13.2.0	-Ofast -march=znver2 -mtune=znver2	-Ofast -mcpu=neoverse-v1
	clang 18.1.3	-Ofast -march=znver2 -mtune=znver2	-Ofast -mcpu=neoverse-v1
Ofast, native, no vec.	GCC 13.2.0	-Ofast -march=znver2 -mtune=znver2 -fno-tree-vectorize	-Ofast -mcpu=neoverse-v1 -fno-tree-vectorize
	clang 18.1.3	-Ofast -march=znver2 -mtune=znver2 -fno-slp-vectorize -fno-vectorize	-Ofast -mcpu=neoverse-v1 -fno-slp-vectorize -fno-vectorize
O2, no vec.	GCC 13.2.0	-O2 -fno-tree-vectorize	-O2 -fno-tree-vectorize
	clang 18.1.3	-O2 -fno-slp-vectorize -fno-vectorize	-O2 -fno-slp-vectorize -fno-vectorize

Table 1.2: Compiler versions and compilation flags used for finite element kernel benchmarks.

162 Results for kernel benchmarks are shown in [Figure 1.2](#) and [Figure 1.3](#). Low-order
 163 kernels ([Figure 1.2](#)) show no dependence on compiler vectorisation setup. On the
 164 other hand, AWS c7g shows 1.3x speed-up over Aion which we attribute to higher
 165 memory bandwidth for a single process.

166 High-order kernels (Figure 1.3), which are expected to benefit from SIMD operations,
 167 show a clear link between compiler settings and performance. Both clang and GCC
 168 auto-vectorisers perform well, producing a noticeable speed-up ($>2x$) in the most
 169 optimised setting. The vectorisation speed-up ($>4x$) is more significant with the
 170 Aion nodes.

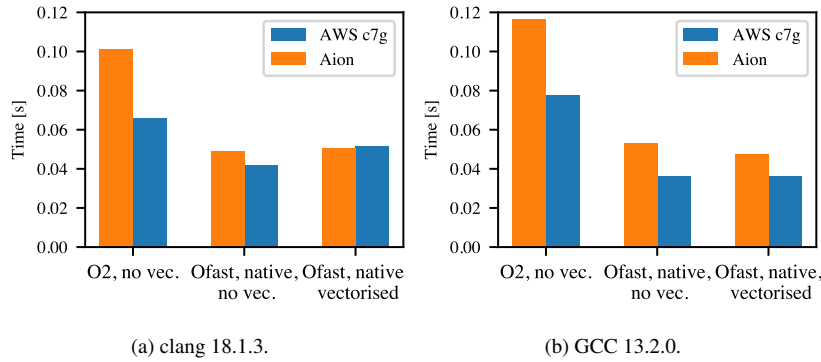


Fig. 1.2: Low-order Laplace operator action assembly.

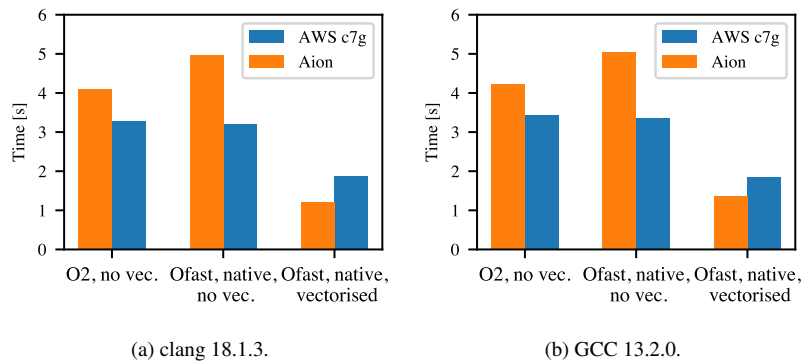


Fig. 1.3: High-order Laplace operator action assembly.

171 Optimisation reports (`-Rpass=loop-vectorize` for clang, `-fopt-info-vec-optimized`
 172 for GCC) and the inspection of the generated assembly reveal that the low-order oper-
 173 ator action the compiler optimisation level `-Ofast` makes constant folding more
 174 effective and pre-computes more operations at compile-time (e.g. partial sums of the
 175 static constant arrays) (Godbolt 2024e).

176 On Graviton3, both GCC and clang generate SVE FMLA instructions (Arm, 2024)
 177 for both the coefficient evaluation and tensor assignment loops (Godbolt, 2024b,a).
 178 FMLA, or Floating-point fused Multiply-Add, is a SIMD instruction that multiplies
 179 two vectors stored in SVE registers and adds the result to a third vector. The coefficient
 180 evaluation loop with no interdependencies between iterations is a perfect example for
 181 compiler auto-vectorisation. Moreover, for coefficients of higher order discretization,
 182 there is potential for exploiting wider SVE registers (up to 2048 bits).

183 An assembly excerpt for the coefficient evaluation is shown below.

```
184 ld1d {z0.d}, p0/z, [x7, x0, lsl #3]
185 ld1d {z25.d}, p0/z, [x3, x0, lsl #3]
186 fmla z3.d, p0/m, z25.d, z0.d
187 ...
188 faddv d1, p1, z1.d
```

191 As expected, there are two contiguous loads LD1D into two of the available SVE Z0-
 192 Z31 registers followed by a fused Multiply-Add instruction. The result is accumulated
 193 into an SVE register Z3 which is then horizontally summed outside of the vectorised
 194 loop (FADDV). Here P0 is a predicate register without any constraints on the available
 195 elements.

196 On Aion, both GCC and clang vectorise both coefficient evaluation and tensor
 197 assignment loops and rely on the VFMADD231PD instructions on the YMM registers,
 198 i.e. vectorisation width of 4 doubles (Godbolt, 2024c,d).

199 **Parallel scalability**

200 Results for the parallel scalability were produced using performance test codes for
 201 FEniCSx (Wells and Richardson, 2023) built against DOLFINx 0.6.0 and PETSc
 202 3.18 (Balay et al., 2023) with the Spack package manager setup to use GCC 12.2.0.
 203 We setup Spack to use a version of OpenMPI provided by AWS which includes
 204 the appropriate libfabric with native support for the EFA interconnect. Libfabric
 205 is a network communication library that abstracts networking technologies from
 206 fabric and hardware implementation, ensuring optimal data transfer across Amazon's
 207 proprietary EFA interconnect.

208 The Poisson equation solver benchmark consists of the following measured steps:

- 209 1. Create mesh. Create a unit cube mesh and discretise using linear tetrahedral cells.
 210 Partition the mesh with Parmetis 4.0.3 partitioner (Karypis and Kumar, 1998)
 211 and distribute.
- 212 2. Assemble matrix. Execute the local Poisson equation kernel over the mesh and
 213 assemble into a PETSc MATMPIAIJ (distributed compressed sparse row) matrix.

214 3. Solve linear system. Run Conjugate Gradient (CG) solver with a classical algebraic
215 multigrid (BoomerAMG (Falgout and Yang 2002)) preconditioner.

216 Creating the mesh (including partitioning), assembling matrices and solving the
217 resulting linear system are typically the most expensive steps in a finite element
218 solve. They also contain significant parallel communication steps that can highlight
219 issues in either the finite element solver, or the underlying MPI hardware/software
220 stack, leading to poor parallel scaling. Weak scaling results (constant workload of
221 approx. 5×10^5 degrees-of-freedom per process) are shown in Figure 1.4. Both Aion
222 and AWS c7gn show almost constant times for mesh creation ($< 5\%$ difference).

223 Matrix assembly is expected to have ideal weak parallel scalability due to the cell-
224 local nature of the assembly loop and negligible amount of MPI communication
225 during matrix finalisation. Aion and AWS c7gn show small increase in time (10-15
226 %) for 512 processes.

227 The time for the solve step increases by 40 % for 512 processes on AWS c7gn and by
228 27 % on Aion. However, the number of Krylov iterations of the preconditioned CG
229 solver grows from 16 to 20 for 512 processes (25% increase) due to the inefficiency
230 of the algebraic multigrid preconditioner on an unstructured 3D mesh. Taking this
231 into account, the time per iteration is almost constant on Aion ($< 5\%$) and a small
232 increase of 15 % on AWS c7gn is observed.

233 Conclusions

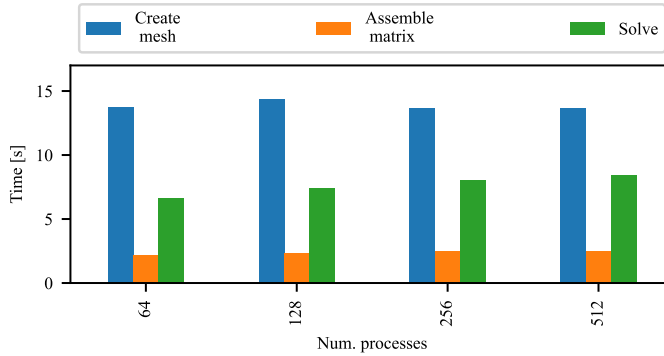
234 Benchmarks for memory bandwidth, local finite element kernels and parallel scala-
235 bility of Poisson solver were executed on Aion nodes and on AWS c7g(n) instances.

236 Memory bandwidth measured using STREAM MPI confirms higher memory trans-
237 fer rate of AWS c7g(n), but a superior total bandwidth of 310 GB s^{-1} per Aion
238 node.

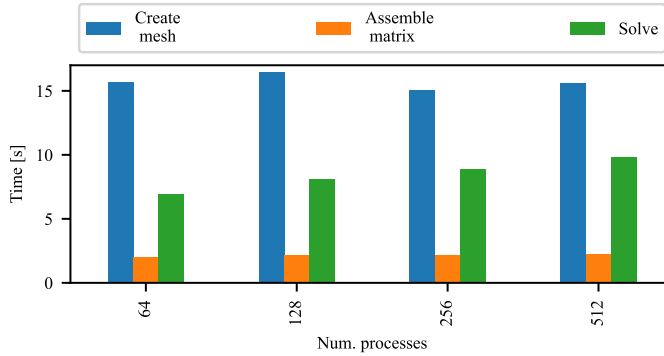
239 In terms of auto-vectorisation capabilities of GCC 13.2.0 and clang 18.1.3, both
240 produced optimised instructions for the targeted microarchitectures (Zen 2 for Aion
241 and Neoverse V1 for AWS c7g). This observation was confirmed with performance
242 benchmarks based on local finite element kernels for the Laplace operator.

243 The MPI-based distributed memory Poisson equation solver shows weak scaling
244 with 15 % time per iteration increase for 512 processes on the c7gn-based cluster.
245 Results for the in-house University of Luxembourg Aion system are slightly superior
246 with almost constant ($< 5\%$ difference) time per iteration for 512 processes.

247 Based on our results, we conclude that AWS Graviton3 instances are a viable alter-
248 native for high-performance computing tasks using the FEniCS Project automated
249 finite element solver. These instances are likely to be particularly interesting for users



(a) Aion, 5×10^5 degrees-of-freedom per process, 25 % utilisation (32 processes per node).



(b) AWS c7gn, 5×10^5 degrees-of-freedom per process, 50 % utilisation (32 processes per node).

Fig. 1.4: Weak parallel scalability of the DOLFINx Poisson equation solver on Aion and AWS c7gn systems.

250 with infrequent or highly elastic large-scale computational demands [Emeras et al.](#)
 251 [\(2016\)](#).

252 In future work we plan to work on other more complex problems (e.g. linear elastic-
 253 ity) and performance benchmarks of direct solvers. Additionally, the latest generation
 254 Graviton4 instances provide an improved Neoverse V2 instruction set, which has a
 255 smaller SVE vector length of 128 bits, [\(Arm 2025\)](#), which warrants further investi-
 256 gation.

257 **Supplementary material**

258 Raw data and plotting scripts are archived at (Habera and Hale 2025).

259 **Acknowledgements** This project has received compute resources from Amazon Web Services
 260 (AWS) through the first and second collaborative University of Luxembourg and AWS Graviton3
 261 call. The experiments presented in this paper were carried out using the HPC facilities of the
 262 University of Luxembourg (Varrette et al. 2022) – see <https://hpc.uni.lu>

263 This research was funded in whole, or in part, by the National Research Fund (FNR), grant reference
 264 COAT/17205623. For the purpose of open access, and in fulfillment of the obligations arising from
 265 the grant agreement, the author has applied a Creative Commons Attribution 4.0 International (CC
 266 BY 4.0) license to any Author Accepted Manuscript version arising from this submission.

267 **References**

- 268 Alnæs MS, Blechta J, Hake JE, Johansson A, Kehlet B, Logg A, Richardson C, Ring J, Rognes
 269 ME, Wells GN (2015) The FEniCS Project Version 1.5. Archive of Numerical Software 3,
 270 doi:[10.11588/ans.2015.100.20553](https://doi.org/10.11588/ans.2015.100.20553)
- 271 Alnæs MS, Logg A, Ølgaard KB, Rognes ME, Wells GN (2014) Unified Form Language: A
 272 Domain-specific Language for Weak Formulations of Partial Differential Equations. ACM
 273 Trans Math Softw 40(2):9:1–9:37, doi:[10.1145/2566630](https://doi.org/10.1145/2566630), URL <http://doi.acm.org/10.1145/2566630>
- 274 Arm (2024) Arm Architecture Reference Manual for A-profile architecture. <https://developer.arm.com/documentation/ddi0487/ka> [Accessed 11-09-2024]
- 275 Arm (2025) Arm neoverse v2 core technical reference manual. <https://developer.arm.com/documentation/102375/latest/> [Accessed 11-01-2025]
- 276 Balay S, et al. (2023) PETSc Web page. URL <https://petsc.org/>
- 277 Baratta I, Richardson C, Dokken JS, Hermano A (2023a) Local Finite Element Operator Bench-
 278 marks. URL https://github.com/IgorBaratta/local_operator
- 279 Baratta IA, Dean JP, Dokken JS, Habera M, Hale JS, Richardson CN, Rognes ME, Scroggs
 280 MW, Sime N, Wells GN (2023b) DOLFINx: The next generation FEniCS problem solving
 281 environment. doi:[10.5281/zenodo.10447666](https://doi.org/10.5281/zenodo.10447666)
- 282 BCS (2025) Specs - Bristol Centre for Supercomputing Documentation — docs.isambard.ac.uk.
 283 <https://docs.isambard.ac.uk/specs/> [Accessed 12-01-2025]
- 284 Emeras J, Varrette S, Bouvry P (2016) Amazon Elastic Compute Cloud (EC2) vs. In-House HPC
 285 Platform: A Cost Analysis. In: 2016 IEEE 9th International Conference on Cloud Computing
 286 (CLOUD), pp 284–293, doi:[10.1109/CLOUD.2016.0046](https://doi.org/10.1109/CLOUD.2016.0046) URL <https://ieeexplore.ieee.org/document/7820283>
- 287 Falgout RD, Yang UM (2002) hypre: A Library of High Performance Preconditioners. In: Sloot
 288 PMA, Hoekstra AG, Tan CJK, Dongarra JJ (eds) Computational Science — ICCS 2002, no. 2331
 289 in Lecture Notes in Computer Science, Springer Berlin Heidelberg, pp 632–641, doi:[10.1007/3-540-47789-6_66](https://doi.org/10.1007/3-540-47789-6_66)
- 290 Fujitsu (2024) Supercomputer Fugaku retains first place worldwide in HPCG and Graph500
 291 rankings — fujitsu.com. <https://www.fujitsu.com/global/about/resources/news/press-releases/2024/1119-01.html> [Accessed 10-01-2025]
- 292 Godbolt M (2024a) Compiler Explorer - (ARM64 gcc 13.2.0). <https://godbolt.org/z/sxGo17Wq9> [Accessed 11-09-2024]
- 293 Godbolt M (2024b) Compiler Explorer - high-order (armv8-a clang 18.1.0). URL <https://godbolt.org/z/WzYEefEGK> [Accessed 11-09-2024]

- 302 Godbolt M (2024c) Compiler Explorer - high-order (x86-64 clang 18.1.0). <https://godbolt.org/z/fEz64zzWx> [Accessed 11-09-2024]
- 303
- 304 Godbolt M (2024d) Compiler Explorer - high-order (x86-64 gcc 13.2). <https://godbolt.org/z/aYeYcb6z1> [Accessed 11-09-2024]
- 305
- 306 Godbolt M (2024e) Compiler Explorer - low-order (armv8-a clang 18.1.0). <https://godbolt.org/z/4Mdbvndrf> [Accessed 11-09-2024]
- 307
- 308 Google (2025) Arm VMs on Compute — Compute Engine Documentation — Google Cloud — cloud.google.com. <https://cloud.google.com/compute/docs/instances/arm-on-compute> [Accessed 12-01-2025]
- 309
- 310 Habera M, Hale JS (2025) Supplementary material: The FEniCS Project on AWS Graviton3. doi:[10.5281/zenodo.13748404](https://doi.org/10.5281/zenodo.13748404)
- 311
- 312 Karypis G, Kumar V (1998) A fast and high quality multilevel scheme for partitioning irregular graphs. *SIAM Journal on Scientific Computing* 20(1):359–392. doi:[10.1137/s1064827595287997](https://doi.org/10.1137/s1064827595287997). URL <http://dx.doi.org/10.1137/S1064827595287997>
- 313
- 314 Kirby RC, Logg A (2006) A Compiler for Variational Forms. *ACM Trans Math Softw* 32(3):417–444. doi:[10.1145/1163641.1163644](https://doi.org/10.1145/1163641.1163644). URL <http://doi.acm.org/10.1145/1163641.1163644>
- 315
- 316 McCalpin JD (1991-2007) STREAM: Sustainable memory bandwidth in high performance computers. Tech. rep., University of Virginia, Charlottesville, Virginia, URL <http://www.cs.virginia.edu/stream/>
- 317
- 318 McCalpin JD (1995) Memory Bandwidth and Machine Balance in Current High Performance Computers. IEEE Computer Society Technical Committee on Computer Architecture (TCCA) Newsletter pp 19–25
- 319
- 320 McCalpin JD (2023) The evolution of single-core bandwidth in multicore processors — sites.utexas.edu. <https://sites.utexas.edu/jdm4372/2023/04/25/the-evolution-of-single-core-bandwidth-in-multicore-processors/> [Accessed 10-01-2025]
- 321
- 322 Microsoft (2024) Announcing the preview of new Azure VMs based on the Azure Cobalt 100 processor — Microsoft Community Hub — techcommunity.microsoft.com. <https://techcommunity.microsoft.com/blog/azurecompute/announcing-the-preview-of-new-azure-vms-based-on-the-azure-cobalt-100-processor/4146353> [Accessed 12-01-2025]
- 323
- 324 Rajovic N, Rico A, Mantovani F, Ruiz D, Vilarrubi JO, Gomez C, Backes L, Nieto D, Servat H, Martorell X, Labarta J, Ayguade E, Adeniyi-Jones C, Derradji S, Gloaguen H, Lanucara P, Sanna N, Mehaut JF, Pouget K, Videau B, Boyer E, Allalen M, Auweter A, Brayford D, Tafani D, Weinberg V, Brommel D, Halver R, Meinke JH, Beivide R, Benito M, Vallejo E, Valero M, Ramirez A (2016) The mont-blanc prototype: An alternative approach for hpc systems. In: SC16: International Conference for High Performance Computing, Networking, Storage and Analysis, IEEE, p 444–455. doi:[10.1109/sc.2016.37](https://doi.org/10.1109/sc.2016.37). URL <http://dx.doi.org/10.1109/SC.2016.37>
- 325
- 326 Roche FJ (2023) Evaluation of C++ SIMD Libraries. Bachelor’s thesis, Der Ludwig-Maximilians-Universität München, URL <https://www.mnm-team.org/pub/Fopras/rock23/>
- 327
- 328 Sandia NL (2018) Astra supercomputer at Sandia Labs is fastest Arm-based machine on TOP500 list — sandia.gov. <https://www.sandia.gov/labnews/2018/11/21/astra-2/> [Accessed 10-01-2025]
- 329
- 330 Simakov NA, Deleon RL, White JP, Jones MD, Furlani TR, Siegmann E, Harrison RJ (2023) Are we ready for broader adoption of ARM in the HPC community: Performance and Energy Efficiency Analysis of Benchmarks and Applications Executed on High-End ARM Systems. In: Proceedings of the HPC Asia 2023 Workshops, Association for Computing Machinery, New York, NY, USA, HPCAsia ’23 Workshops, pp 78–86. doi:[10.1145/3581576.3581618](https://doi.org/10.1145/3581576.3581618)
- 331
- 332 Suárez D, Almeida F, Blanco V (2024) Comprehensive analysis of energy efficiency and performance of ARM and RISC-V SoCs. *The Journal of Supercomputing* 80(9):12771–12789. doi:[10.1007/s11227-024-05946-9](https://doi.org/10.1007/s11227-024-05946-9)
- 333
- 334
- 335

- 356 Varrette S, Cartiaux H, Peter S, Kieffer E, Valette T, Ollloh A (2022) Management of an Academic
357 HPC & Research Computing Facility: The ULHPC Experience 2.0. In: Proc. of the 6th ACM
358 High Performance Computing and Cluster Technologies Conf. (HPCCT 2022), Association for
359 Computing Machinery (ACM), Fuzhou, China, doi:[10.1145/3560442.3560445](https://doi.org/10.1145/3560442.3560445)
- 360 Wells G, Richardson C (2023) Performance test codes for FEniCSx. URL:[https://github.com/
361 FEniCS/performance-test](https://github.com/FEniCS/performance-test)